Journal of Molecular Liquids 392 (2023) 123460

Contents lists available at ScienceDirect

Journal of Molecular Liquids

journal homepage: www.elsevier.com/locate/molliq

Ionic liquid/metal salt mixtures at the graphene interface: A density functional theory approach

Alejandro Rivera-Pousa [a,b], José M. Otero-Mato [a], Carlos Damián Rodríguez-Fernández [a,c], Kazem Zhour [d], Hadrián Montes-Campos [a,b,e,*], Trinidad Méndez-Morales [a,b,*], Luis M. Varela [a,b]

[a] Grupo de Nanomateriais, Fotónica e Materia Branda, Departamento de Física de Partículas, Universidade de Santiago de Compostela, Campus Vida s/n, E-15782, Santiago de Compostela, Spain
[b] Instituto de Materiais (iMATUS), Universidade de Santiago de Compostela, Avenida do Mestre Mateo 25, E-15782, Santiago de Compostela, Spain
[c] Departamento de Física e Ciencias da Terra, Universidade da Coruña, Campus de A Zapateira s/n, E-15071, A Coruña, Spain
[d] Institute of Physical Chemistry, University of Münster, Corrensstraße 28/30, 48149, Münster, Germany
[e] CIQUP, Institute of Molecular Sciences (IMS)—Departamento de Química e Bioquímica, Faculdade de Ciências da Universidade do Porto, Rua Campo Alegre, 4169-007, Porto, Portugal

ARTICLE INFO

Keywords:
Ionic liquids
Graphene
Metal atoms adsorption
Density functional theory
Optoelectronic properties

ABSTRACT

The interaction of graphene sheets with metal cations is very relevant because of the modifications that are induced in the electrochemical properties of the 2D material. Ionic liquids are a promising kind of materials with several applications in electrochemical devices, so understanding how they affect the graphene-metal interaction is key for their practical implementation. Therefore, we have studied the adsorption of a mixture of an ionic liquid and a metal salt on a graphene surface by means of first-principles calculations. Several metals were chosen to analyze the effect they have on the optoelectronic properties of the graphene monolayer and to understand the trends in their adsorption behavior. We have characterized the ground state configurations in terms of their binding energies and the distance between the metal atom and the graphene layer. From the analysis of the charge transfer behavior, calcium and magnesium have been identified as the species that transfer the highest and the lowest amount of charge, respectively, which is related to their ionization energies. Band structure diagrams and projected density of states calculations also show that the energy shift of the Dirac cone increases with the degree of charge transfer. In addition, a stronger interaction of magnesium with the ionic liquid compared to that of other metal atoms was observed. The analysis of several electromagnetic parameters indicated an anisotropic behavior for electric fields polarized both perpendicular and parallel to the graphene layer. Our density functional theory study offers fundamental insights into the adsorption behavior of ionic liquids mixed with metal ions on monolayer graphene.

1. Introduction

In recent years, scientific emphasis has been focused on the unique optical, electronic, mechanical and chemical properties of 2D materials [1,2]. Among them, the most studied one is undoubtedly graphene, which has become a central topic of research interest due to its high carrier mobility, extraordinary strength, high thermal conductivity and excellent optical properties [3–5]. All of them can be tuned through different methods like impurity doping, designed defects, adsorption or chemical functionalization [6–11]. This versatility has enabled graphene to hold great potential for a virtually unlimited range of applications, including electronics [12], energy [13], medicine [14], sensors [15] and light processing [16].

An interesting aspect of graphene sheets lies in their interaction with metal cations due to the change in electronic and mechanical properties, thus providing new functionalities and widening their use in many fields. Metals interacting with graphene have been thoroughly studied and analyzed by means of both experimental studies [17–19] and computational calculations based on first-principles density functional theory (DFT) [20–31]. Among the latter, Olsson et al. [32] studied the adsorption and migration of several alkali atoms on pristine and defective graphene surfaces, and they reported more favorable adsorption

* Corresponding authors.
E-mail addresses: hadrian.montes@usc.es (H. Montes-Campos), trinidad.mendez@usc.es (T. Méndez-Morales).

https://doi.org/10.1016/j.molliq.2023.123460
Received 30 June 2023; Received in revised form 29 September 2023; Accepted 29 October 2023
Available online 4 November 2023

energies for Li^+ and K^+ ions than for Na^+. Similarly, Mendoza-Cortes and coworkers [33,34] showed how to modify the electronic properties of bilayer graphene with the intercalation of transition metals. This study found that the Dirac point was pushed down below the Fermi energy level in all the intercalated structures except for vanadium, which had the Dirac cone in its band structure.

Among all the works addressing the adsorption of molecules on a graphene surface, ionic liquids (ILs) are emerging as a relevant field of study due to their attractive properties for a great number of applications. These salts that are mainly composed of cations and anions and have melting points below 100 °C, offer high thermal stability, high ionic conductivity, negligible volatility, and structural and physicochemical tunability through appropriate selection of the ions [35,36]. Because of these benefits, their efficient utilization in synthesis, catalysis, electrochemistry, gas separation, tribology, pharmaceuticals and energy storage devices has been exhaustively tested in the last decades [37–41]. Thus, the growing interest on understanding the adsorption mechanism of ILs on different surfaces has led to numerous experimental investigations in this area [42–44]. Alongside the experimental efforts, computational methods such as those based on electronic structure have been widely employed to analyse the properties and interactions of ILs with a large panel of surfaces, including graphene (or its derivatives) and other 2D materials [45–49], polycyclic aromatic hydrocarbons [50,51], and metal interfaces [52–54]; with the purpose of elucidating their influence on the electronic properties of the surface [55–59], and evaluate their potential use in applications such as exfoliation [60–62] or energy storage devices [63–68]. For example, Kamath and coworkers [57–59] performed a series of calculations to compare the adsorption characteristics of different ILs on graphene, defective graphene and fluorographene surfaces. They observed that the presence of defects on the graphene nanoflakes increases the binding energy of ILs by about 10% in comparison with pristine graphene and hexagonal boron-nitride nanosheets. However, fluorinated graphene strongly decreases the binding energy compared to them.

Nevertheless, even though ILs are promising electrolytes for energy storage devices, there is still scarce information about their interfacial interactions with graphene substrate and the electronic structure upon adsorption when it comes to their mixtures with metal atoms. Up to our knowledge, there is only one publication in which the effect of the adsorption of an imidazolium-based IL mixed with a potassium salt on the electronic and optical properties of graphene and borophene was considered [69]. The authors reported a downward shift of the Dirac cones relative to their Fermi level for both structures due to the electron transferred from potassium to the 2D-materials. Also, they observed that the presence of the IL increased the charge transferred from the metal atom to the graphene/borophene sheets when compared to its adsorption on pristine materials.

Thus, in this work a comprehensive investigation was carried out by means of DFT simulations to shed some light on the interaction mechanism between IL-metal salt mixtures and the graphene substrate. This computational technique was chosen due to its capability of producing highly accurate results that can be compared to experimental findings [70,71] and because it takes into account interactions that are not accessible by means of other techniques such as MD. The screening of several metal atoms (lithium (Li), sodium (Na), magnesium (Mg), calcium (Ca), and aluminum (Al)) allowed us to compare the electronic and optical properties avoiding more costly trial-and-error experimental measurements, which is of fundamental importance for optimizing the performance and efficiency of a new generation of electronic, optoelectronic and energy storage devices. The IL employed in this study was 1-butyl-3-methylimidazolium tetrafluoroborate ([BMIM][BF_4]), which was chosen with the purpose of comparison with the same hybrid system doped with potassium that was previously reported by some members of our group [69]. Also, the potential of this IL as a suitable electrolyte (pure or in mixtures) for energy storage devices such as supercapacitors or lithium-ion batteries has been often considered [72,73].

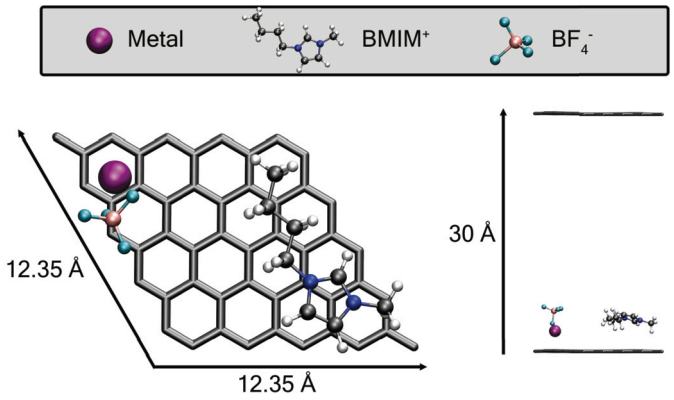

Fig. 1. Top and side views of a snapshot of one of the simulated systems.

In this study, we investigate the role played by the metal atoms doping the IL in the adsorption mechanism and the interaction with monolayer graphene. Of particular interest is to understand the effect of their atomic radius or valence on several electronic and optical properties, such as binding energy, charge transfer, electron density difference (EDD), band structure, partial density of states (PDOS), real and imaginary dielectric functions (ε), electron energy loss function (EELS, L), real and imaginary refractive index (n), reflectivity (R) and absorption coefficient (α). All the optical properties are studied for parallel and perpendicular (to the graphene layer) incoming electromagnetic radiation.

The paper is organized as follows: the details of the computational and theoretical methodology are given in Section 2, the results are presented and discussed in Section 3, and finally, in Section 4 we summarize our main conclusions.

2. Simulations details

In this work, we performed DFT calculations to study the effect of the adsorption of a metal atom in a system composed of a 2D graphene layer with an IL ([BMIM][BF_4]) already adsorbed. We explored 5 different metal species (lithium, sodium, magnesium, calcium and aluminum) to unveil the effect of properties such as atomic radius or valence. All calculations were conducted using Quantum-ESPRESSO (QE) package [74–76], which is based on plane wave pseudopotentials. For all the calculations in this work, we used the ultrasoft pseudopotentials. To describe the electron exchange-correlation energy, we employed the generalized gradient approximation (GGA) of Perdew-Burke-Ernzerhoff (PBE) [77]. Cutoffs of 50 Ry and 400 Ry in kinetic energy and charge density were deemed sufficient to achieve proper convergence.

A 5×5 supercell for graphene (2.47 Å lattice constant) was chosen as it approximately covers the surface of one anion-cation pair of the IL, comprising a total of 50 carbon atoms. This graphene layer was set up perpendicular to the z-axis. To ensure proper decoupling from periodic replicas, a buffer spacing of 30 Å in the z-direction was established. After a relaxation of the system, the IL was placed in the cell according to previous molecular dynamics (MD) simulations [78]. Another relaxation was carried out, and then the metal atom was added to the resulting configuration. We therefore had 5 equivalent systems (graphene/IL/metal) that were all of them relaxed once again. A snapshot of one of these systems is shown in Fig. 1.

Self consistency threshold was set to 10^{-6} Ry. In order to efficiently sample the Brillouin zone of the different structures, Methfessel-Paxton smearing [79] was used in conjunction with a 20×20×1 Γ-centered k-point mesh and a gaussian spreading of 0.01 Ry. It was checked in previous works performed by our group [55,69] that tightening the threshold and/or the k-points criteria does not lead to remarkable differences in

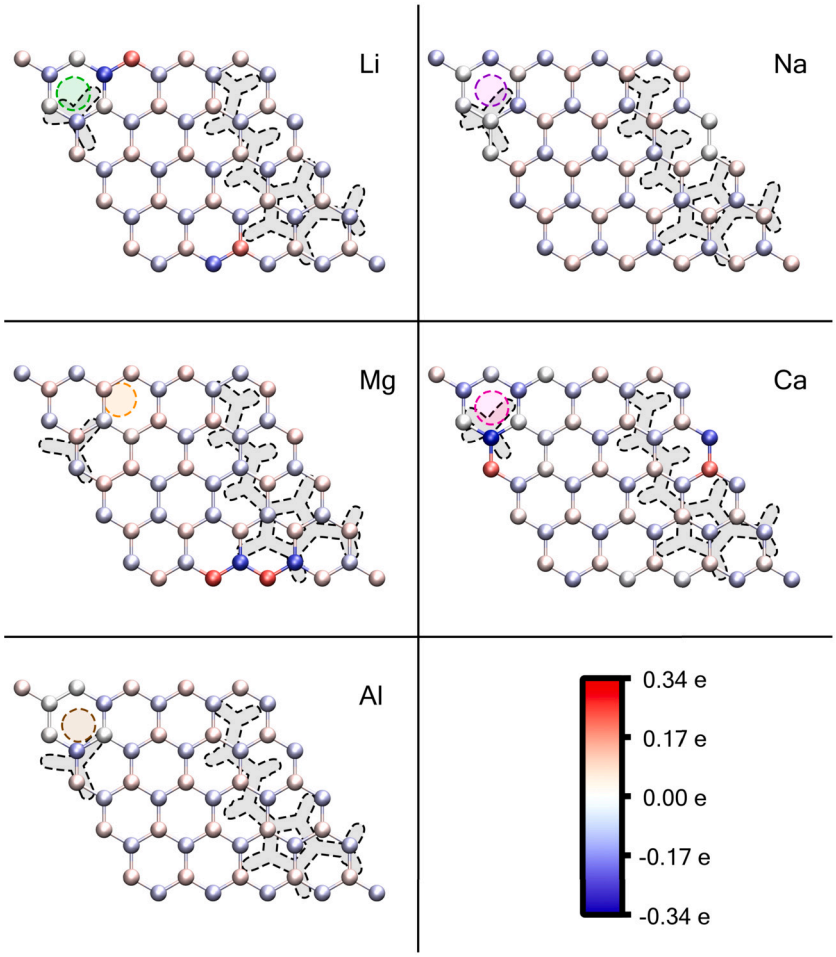

Fig. 2. Charge of the carbon atoms of graphene induced by the presence of the IL and the different metals calculated using Bader charge analysis. Dashed outlines show the position of the IL and the corresponding metal in each system. The respective sizes of the metals have been increased for clarity purposes.

the obtained results. The same mesh was also used for the density of states (DOS) calculations. However, norm-conserving pseudopotentials in a 7×7×1 mesh disposition were employed for the computation of optical properties. These properties can all be derived from the complex dielectric function as described in Refs. [55,69]. As the first Brillouin zone of the considered system is hexagonal, the most convenient path to explore for the band structure, according to the corresponding high symmetry points, is the Γ → M → K → Γ path, along 91 different k-points. This choice is well-established in the literature [80–84], as it is commonly used in studies of band structures for graphene and related structures. In order to obtain the charge of the atoms, Bader charge analysis [85] was employed, and the necessary .cube file was obtained with Quantum Espresso's pp.x code.

Table 1
Total charge of the different species after Bader analysis of the relaxed configurations. Values for simulations with K obtained from Ref. [69] are included for comparison. First and second ionization energies (IE, in eV) for each element from Ref. [86] are also included.

	Charge (e)				Ionization energy	
System	Graphene	IL cation	IL anion	Metal	1st IE	2nd IE
G/IL/Li	-0.90	0.95	-0.95	0.90	5.39	75.64
G/IL/Na	-0.91	0.94	-0.94	0.90	5.14	47.29
G/IL/Mg	-0.20	0.88	-1.01	0.32	7.65	15.03
G/IL/Ca	-1.46	0.85	-0.91	1.52	6.11	11.87
G/IL/Al	-0.86	0.95	-1.16	1.07	5.99	18.83
G/IL/K	-0.91	0.95	-0.94	0.90	4.34	31.63

3. Results and discussion

3.1. Electronic properties

A Bader charge analysis [85] was carried out in order to determine the induced charge transfer to the graphene surface atoms that emerges from the adsorption of the IL and a metal atom. In Fig. 2 we can observe that there is a redistribution of electric charge in the graphene sheet when compared with the metal absent configuration [55]. The most remarkable feature is that Li and Ca atoms induce high polarity in some of their close neighboring carbons. In the case of Mg, a high induced polarization is also observed in some carbon atoms, which is originated not only from the presence of the metal but also from that of the IL ions, since the three of them are located at the same distance from the 2D surface. On the other hand, the presence of Na and Al leads to a more homogeneous distribution of the charge, as it was also previously observed for K [69]. However, a situation in which every positively charged site is surrounded by negatively charged carbon atoms was only predicted for lithium. As it can be seen in Table 1, in general the metal is the species that transfers approximately all its charge to the graphene sheet, while the IL ions suffer almost no modification and keep their bulk charge of ±1e. However, a detailed comparison between the charge of cation and anion in the different systems after adsorption indicates that the cation always tends to become less positive, whereas the anion usually tends to be less negative except for mixtures with magnesium and, mainly, with aluminum, where it gains charge. Moreover, the total transfer of charge from magnesium to graphene is predictably

Table 2
Binding energy (ΔE) and distance between the metal atom and i) its nearest carbon atom (d_{MC}), ii) the center of mass of the anion (d_{MA}), iii) the center of mass of the imidazolium ring (d_{MR}), and iv) the terminal carbon of the imidazolium tail (d_{MT}) for each of the studied systems. Values for simulations with K obtained from Ref. [69] are included for comparison.

	ΔE (eV)	d_{MC} (Å)	d_{MA} (Å)	d_{MR} (Å)	d_{MT} (Å)
G/IL/Li	-3.21	1.97	2.48	6.17	5.34
G/IL/Na	-2.40	2.37	2.83	6.18	5.53
G/IL/Mg	-0.76	4.63	3.25	7.47	5.38
G/IL/Ca	-2.89	2.11	2.95	6.36	5.60
G/IL/Al	-2.20	2.59	3.12	6.23	5.36
G/IL/K	-2.25	2.69	3.18	6.64	5.60

low, which can be explained in terms of the ionization energies (IE) included in Table 1, and from where it can be inferred that only those atoms whose first IE are close to or lower than approximately 6 eV are able to transfer an electron to graphene. In particular, Mg has a stable closed-shell configuration, which explains its large first IE and the difficulty to remove an electron. On the other hand, calcium and, specially, aluminum atoms, despite being located in a more advantageous position than Mg, do not transfer all their free electrons to the graphene. In the first case, Ca has the smallest second IE, which explains the fact that this metal transfers the largest amount of charge to the surface. However, the second IE is still too high for removing two electrons from Ca. For Al, after losing one electron, it achieves a stable electron configuration. Thus, the first electron is relatively easy to remove from aluminum, but the second one is much more difficult to remove from the 1+ charge-state aluminum ion.

We have also calculated the binding energies (ΔE) of the metal atoms on a graphene sheet with an IL already adsorbed on it as

$$\Delta E = E_{G/IL/M} - E_{G/IL} - E_M, \quad (1)$$

where $E_{G/IL/M}$ is the total energy of the graphene layer with the adsorbed IL and the metal atom, $E_{G/IL}$ is the total energy of the graphene layer with the adsorbed IL, and E_M is the total energy of the isolated metal atom. Following these criteria, a negative binding energy is associated to a stable configuration, whereas a positive one is an indication of an unfavorable adsorption on the assembly graphene/IL and the metal atom preferring to remain in its atomic state.

Adsorption energies and structural properties such as the distance between the metal atom and i) its nearest carbon atom (d_{MC}), ii) the center of mass of the anion (d_{MA}), iii) the center of mass of the imidazolium ring (d_{MR}), and iv) the terminal carbon of the imidazolium tail (d_{MT}) are summarized in Table 2. All the metal atoms lie at a distance of about 2 Å from the graphene sheet except magnesium, which is further away from the surface. For visual reference, see Fig. S1 of the Supporting Information, which contains snapshots of all the systems. This is likely related to the lower binding energy of this particular metal in comparison with the rest. In this way, the magnesium atom accommodates itself in the same plane as the IL components, but at a further straight line distance from them than the other metals. However, all the other systems share a quite similar geometrical disposition, with the metal being placed between the graphene sheet and the BF_4^- anion. In addition, we can observe that lithium is the atom more strongly adsorbed on the surface in the presence of the IL, which is in agreement with trends previously reported for the adsorption of metal atoms on pristine graphene [24,32,87]. These observations are coherent with the previous charge transfer analysis. Indeed, Mg is the species located the furthest from the surface because of its vanishing charge transfer ability. For this metal it is not energetically favorable to stay in this electronically highly reactive region, whereas the rest of the metals are located close to graphene because they are capable of transferring electrons to it. Some degree of charge transfer from the Mg atom at distances longer than 4 Å has been previously reported in the presence of an ionic liquid [88].

The electronic behavior was further examined through the charge density difference ($\Delta\rho$) defined as

$$\Delta\rho = \rho_{G/IL/M} - \rho_{G/IL} - \rho_M, \quad (2)$$

where $\rho_{G/IL/M}$, $\rho_{G/IL}$ and ρ_M are the total charge densities of the relaxed system with IL and metal adsorbed on graphene, the system with IL adsorbed on the 2D surface and the isolated metal, respectively. Lateral views of the charge density differences for the different metals are provided in Fig. 3. An isovalue of $\pm 0.017\ e/Å^3$ was considered for the calculation of the diagrams, in which the electron gain and loss configurations are represented by blue and red isosurfaces, respectively. Top views of the same systems are included in the Supporting Information (Fig. S2).

Charge densities of the systems presented in Fig. 3 indicate that the addition of metal atoms modifies not only the electron distribution in the anion and the cation, but also that of the C atoms of graphene lying below the metals. The effect on electronic density difference is similar for all the systems, with metal atoms acquiring an electron loss configuration and C atoms around them showing gain of electrons, as indicated by the red isosurface covering all the metals and the blue one accumulated below them, respectively. This ionic interaction is consistent with the picture previously reported for potassium [69]. Moreover, this effect affects both sides of the surface layer in the systems that showcase greater charge transfer, specially in the case of calcium.

Before starting the analysis of the electronic states of the system, we must take into account that the system is composed of two clearly differentiated parts. The first one is the solid region, which is composed by the graphene and contains the free electrons. The second one is the molecular region, which is composed by the ionic liquid and the metal atom. The difference between these regions is not only a matter of denomination, but they require different tools for their analysis. Therefore, we will first analyze the band structure of the system, focusing on the graphene. Then, we will analyze the highest occupied molecular orbital (HOMO) and the lowest unoccupied molecular orbital (LUMO) of the molecular region and we will use these values to analyze the possible charge transfer between both regions.

The band structure diagrams for all the metals adsorbed on the G/IL systems are shown in Fig. 4, in which the energies are relative to the Fermi level. In order to determine the effect of the metal atoms on the electronic structure, band structure diagrams of pristine graphene are also depicted (black lines) and, for the sake of comparison, they are shifted in such a way that the Dirac cones of both configurations are overlapped. As it is well known, graphene is a semimetal whose conduction and valence bands meet at the Dirac points. On the other hand, it was previously reported that the Dirac cones at the Fermi energy of this 2D material do not suffer any shift upon adsorption of this IL [55]. As it can be seen in Fig. 4, in all cases the adsorption of metal atoms downshifts the Dirac cone below the Fermi level, thus confirming that the charge is donated from the metal to the graphene surface. Therefore, all the metal atoms act like n-type dopants. We can also observe that the band structure of the pristine graphene is approximately conserved in most of the systems. For example, in Fig. 4, where the band structure of the configuration with Mg is represented, the bands corresponding to the periodic part of the system completely coincide, whereas the bands with new molecular levels arise in the form of horizontal bands. In the opposite way, Ca shows to be the atom that induces a larger modification of the bands associated with the periodic part, as it is the metal that transfers the largest amount of charge to the graphene surface. This analysis of the band structure diagrams is also indicative of the degree of charge transfer resistance of these systems and how it varies with the metal atom of the electrolyte.

To analyze this effect, the energy shifts as a function of the charge of the 2D layer are plotted in Fig. 5. There, we can observe that the greater

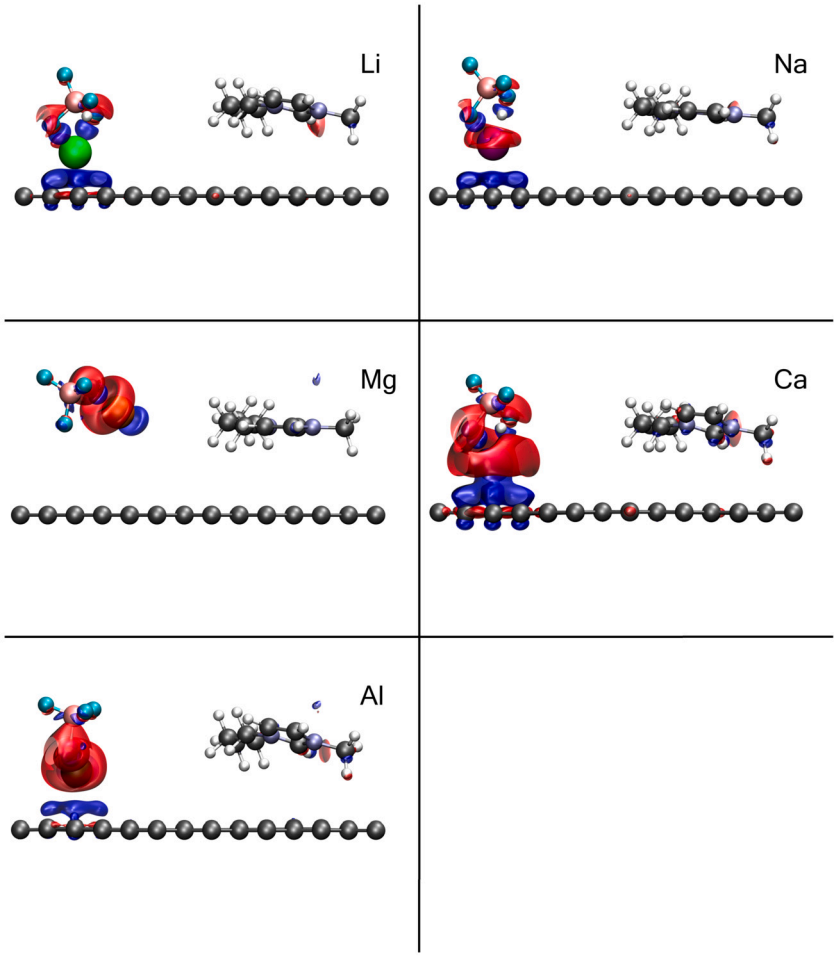

Fig. 3. Lateral views of the electronic density difference between the system with metal and IL, and the system with no metal and the system with only metal. Regions depicted in red/blue correspond to isosurfaces of value $\pm 0.017\ e/Å^3$, and therefore represent electron depletion/accumulation, respectively. The respective sizes of the metals have been increased for clarity purposes.

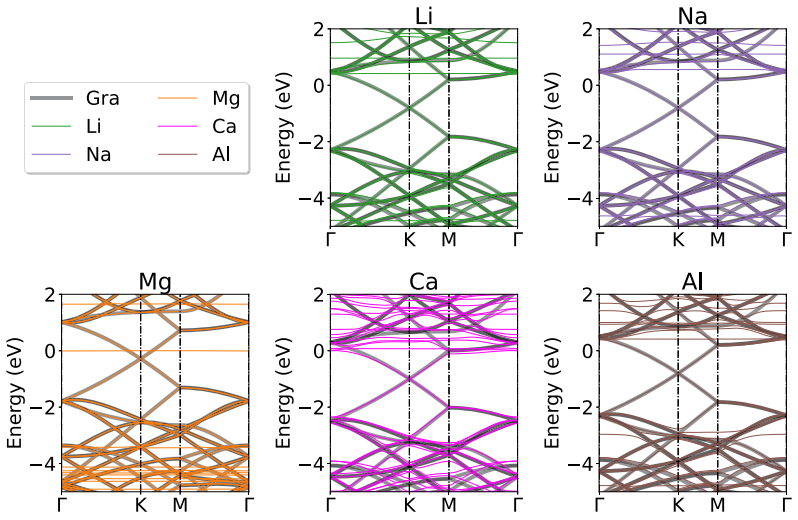

Fig. 4. Band structure diagrams of the different systems, in which the Fermi energy is taken as a reference for the energy level. In a wider black line, the band structure of pristine graphene is positioned so that the Dirac cones are overlapped.

the degree of charge transfer, the larger the shift in energy, confirming the direct relationship. Previously reported values for K [69] are similar to those of Li, Na and Al; whereas Ca and Mg atoms tend to have the largest and the smallest electron transfer and energy shifts, respectively.

To further understand the effect of mixtures of [BMIM][BF_4] and that of the metal atoms on the electronic structure of graphene, we calculated the total (DOS) and projected density of states (PDOS) of the different systems, which are shown in Fig. 6 for energies values relative

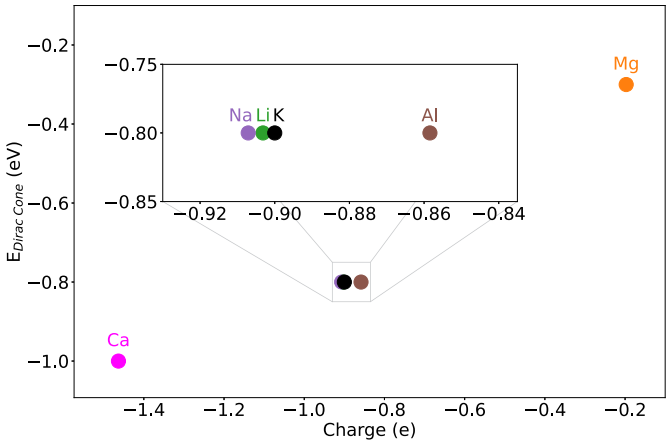

Fig. 5. Energy shift of the Dirac cone as a function of the charge transferred to the graphene surface for each system. For clarity purposes, a zoom was added as an inset to facilitate the view of some points. Values for simulations with K obtained from Ref. [69] are included for comparison.

to the Fermi level within the range $[-5, +5]$ eV. Molecular HOMO-3, HOMO-2, HOMO-1, HOMO, LUMO, LUMO+1, LUMO+2 and LUMO+3 states are also represented and, since some of them are overlapping, each of the energy levels are included in Table S1 of the Supporting Information (the color-code shows to which species the state belongs). In addition, DOS and PDOS within an energy interval of $[-20, +6]$ eV are also included in the Supporting Information (Fig. S3), where it can be seen that the states of both the anion and the cation of the IL notably contribute to the valence states of the systems. For each system, we can easily distinguish the Dirac point, at which the DOS is zero. Below the Fermi level the DOS is almost equivalent to that of graphene up to energies around -3 or -4 eV (depending on the system), where the HOMO level of $[BMIM]^+$ cation (which shows the characteristic "flatline" behavior of molecular systems) lies, and, for mixtures with magnesium and aluminum, also a state of the metal. For mixtures with Mg, this state is superposed with states from the IL ions, and they lie approximately at the Fermi level, which is also very close to the Dirac point. Still, the Dirac point is clearly visible. Due to this feature, we could consider Mg as an interesting option for electronic devices, but it must be remembered that this is the atom adsorbed at the longest distance from the graphene surface. The system with Ca also forms a state at its Fermi level, but in this case it belongs to the IL cation. For the other three systems, the states between the Dirac point and the Fermi level are mostly from graphene. States for Li, Na and Ca lie at approximately 1.6, 1.5 and 0.4 eV above the Fermi energy, respectively, all of them being unoccupied. Moreover, Al has its *3s* and *3p* states at around -3 and 1 eV, respectively. This valence *p* peak being above the Fermi level confirms that close to one electron is transferred from Al to the 2D surface. Notice that a core assumption of PDOS is the projection of the total states on atomic orbitals. In the case of Ca, the dense electronic cloud surrounding it overlaps with that of graphene, as seen in Fig. 3. Therefore, this projection is hampered and this approximation becomes less accurate. As a result, although the total DOS does reflect the presence of the Dirac cone in this system (as previously seen in the band structure in Fig. 4), some states corresponding to the graphene PDOS near the Dirac cone are missing.

The stability and interaction strength of the metal adsorbed on the G/IL system can be explored through the HOMO and LUMO orbitals, which are represented in Figs. S4 and S5 of the Supporting Information, respectively, with the aim of providing a graphical perspective of the orbitals involved. This was calculated by locally integrating the DOS in an energy band around the HOMO and LUMO states, respectively. The energy difference between these orbitals is known as the HOMO-LUMO energy gap, ΔE_{HL}, and can be calculated as

$$\Delta E_{\mathrm{HL}} = E_{\mathrm{LUMO}} - E_{\mathrm{HOMO}} \tag{3}$$

Through the DOS we can analyze the changes in ΔE_{HL} due to molecular interactions, which are tabulated in Table 3. From the $\Delta E_{HL} \approx 5$ eV value previously reported by Zhour et al. [55] for $[BMIM][BF_4]$ adsorbed on graphene, our simulations show an increase upon adsorption of lithium or sodium. This increase in the HOMO-LUMO gap is mainly accomplished by a substantial decrease in the HOMO energy. On the other hand, ΔE_{HL} was found to decrease for the other three metals (magnesium, calcium and aluminum), which is principally achieved by a remarkable decrease in the LUMO energy. Once again, the more substantial change in the HOMO-LUMO gap energy is observed for magnesium, which indicates a strong interaction of the metal with the IL, and is consistent with magnesium being located in the same plane of $[BMIM][BF_4]$.

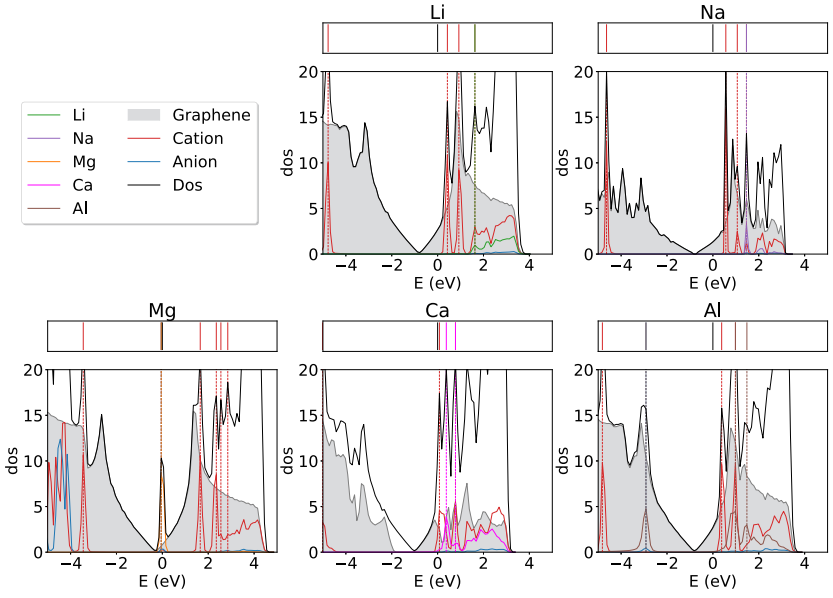

Fig. 6. DOS and PDOS of the different systems. On top of each plot: molecular HOMO-3, HOMO-2, HOMO-1, HOMO, LUMO, LUMO+1, LUMO+2 and LUMO+3 states that are within the considered energy interval. The color indicates to which species the state belongs. Fermi energy is taken as reference for the energy level.

Table 3
HOMO-LUMO energy gap for the different studied systems. Value for simulations with K obtained from Ref. [69] is included for comparison.

	ΔE_{HL} (eV)
G/IL/Li	5.20
G/IL/Na	5.20
G/IL/Mg	1.70
G/IL/Ca	4.70
G/IL/Al	3.30
G/IL/K	5.00

3.2. Optical properties

As mentioned earlier, the adsorption of metal atoms on the G/IL structure modifies the electronic properties of the system, which, in turn, leads to completely different optical characteristics. In this section, we investigate several electromagnetic parameters such as the dielectric constant (ε), the electron energy loss spectrum (EELS, L), refractive index (n), extinction coefficient (κ), reflectivity (R) and absorption coefficient (α) for the perpendicular and parallel polarization to the graphene layer, which are of fundamental importance for many technological applications. The considered frequency interval for the calculation of the optical parameters is taken from 0 to 20 eV, and the corresponding graphs are included in Figs. 7 and 8. In addition, since the visible range is of particular interest, in Figs. S6 and S7 of the Supporting Information only the region between 1.63 and 3.26 eV is plotted.

The dielectric coefficient is a complex magnitude, $\varepsilon(\omega) = \varepsilon_1(\omega) + i\varepsilon_2(\omega)$, whose real and imaginary parts are related through the conventional Kramers-Kronig relations [89]. The former is related to the amount of energy stored by the system, whereas the latter is related to its dissipation of energy. From this function, the refractive index, extinction coefficient, reflectivity and absorption coefficient can be easily calculated as it was explained in detail elsewhere [55,69,90,91].

The real and imaginary parts of the dielectric coefficient as a function of the frequency for all the considered structures are shown in Fig. 7 for both perpendicular and parallel incident electric field. We can clearly observe an anisotropic behavior of this magnitude for the different polarizations of light. In particular, this figure shows that for parallel electric field, the excitations, which are indicated by the peaks of ε_2, are located in the low-energy region. On the contrary, they are mainly observed in the high-frequency one for perpendicular electric field, except for Mg that also has an excitation energy at 2.85 eV. Thus, when the polarization of the electric field is parallel, the imaginary part for Li, Na and Al shows a similar behavior to that previously reported for K [69], with the metals screening the peaks of G/IL below the visible range. However, both Ca and Mg exhibit very intense transitions in this regime. Concerning the perpendicular polarization, a small peak is observed near zero due to the adsorption of Ca and, in addition to the aforementioned peak for Mg, Al shows that some transitions are possible at energies around 5 eV. Then, all the systems have excitation energies situated at around $(10-11)$ eV and 14 eV, thus confirming that the transitions associated to the out-of-plane polarization are prevalent at higher energies.

Focusing now on the real part of the dielectric function, Fig. 7 indicates that for the perpendicular electric field the changes are detected for Ca, Mg and Al at the same energies as for the imaginary one. In the case of in-plane polarization, remarkable modifications compared to the G/IL system are observed at low frequencies mainly for Li, Na and Al, since their curves do not take positive values, contrary to what was previously observed for K [69]. By definition, the plasma frequency is the one at which the real part of the dielectric function cancels, $\varepsilon_1(\omega_p) = 0$. At these frequencies, ε_1 changes its sign [92] and this behavior corresponds to the collective excitations of the electrons. Thus, in Fig. 7

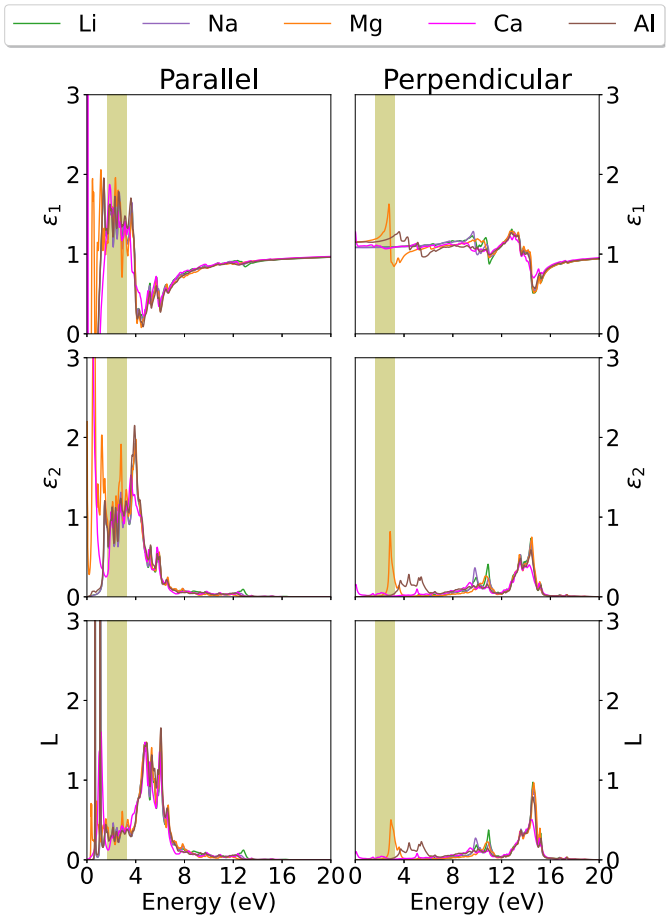

Fig. 7. Real (ε_1) and imaginary (ε_2) parts of the dielectric function and EELS (L) for the different systems with parallel (left) and perpendicular (right) electric field. Shaded stripes represent the optical region.

we can see that for perpendicular polarization there are no plasma frequencies, whereas for parallel polarization three plasma frequencies are induced by the presence of Mg at the interface, two by Ca and one by the rest of the metals. This shows that there are no collective excitations for perpendicular polarization but, for parallel one, the systems absorb the incoming electromagnetic radiation [92].

In Fig. 7 it can be also noticed that the static dielectric constant, which is the real part of the dielectric function at zero frequency, $\varepsilon_1(0)$, is remarkably modified by the adsorption of the metal with respect to the configuration G/IL [55] under in-plane polarization of the electric field. This can be due to an increase in the number of free electrons by the addition of the metal [92], which plays an important role for parallel polarization and implies that the metal-doped system dissipates more energy. On the other hand, for out-of-plane polarization, $\varepsilon_1(0)$ shows quite similar behavior compared to the G/IL system. In particular, it remains unchanged for Li and Na (1.08 and 1.09, respectively), it is slightly increased for Al and Mg (1.15 and 1.16, respectively), and takes the largest value (1.28) when Ca is adsorbed.

The EELS (L), which provides us with information about the collective excitation of the electrons, is also depicted in Figs. 7 and S4 for parallel and perpendicular polarization. The peaks in $L(\omega)$ correspond to 2D plasmons and are due to intraband transitions. Under in-plane electric field, two peaks appear at 0.65 and 1.15 eV (in a similar way to what was found for K [69]), as expected, since they correspond to the dips in the dielectric function. The first one is for Li, Na and Al, whereas the second one is also registered for Ca. For its part, the adsorption of Mg also causes a peak at lower energies (0.35 eV). For out-of-plane elec-

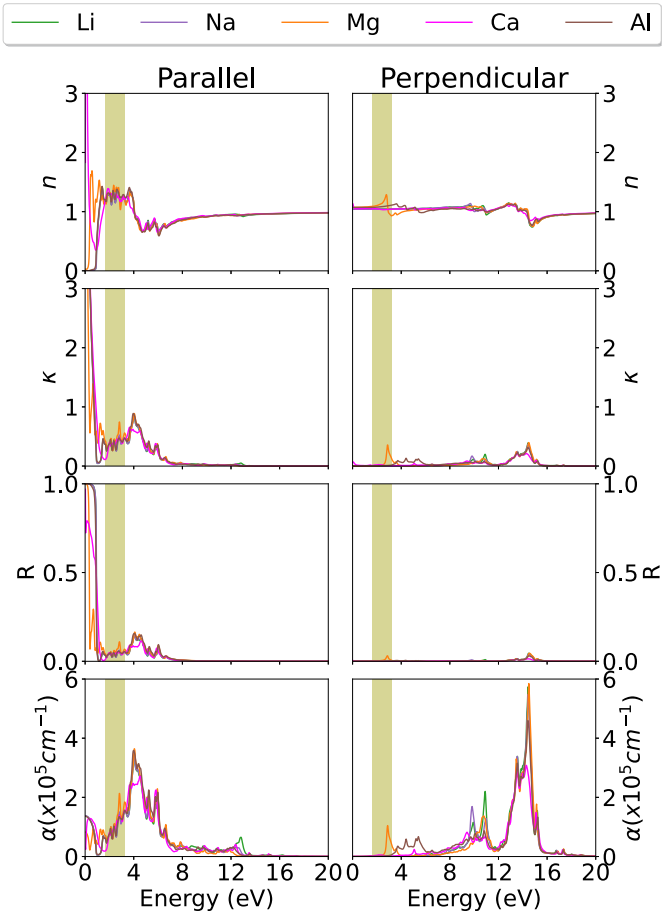

Fig. 8. Refractive index (n), extinction coefficient (κ), reflectivity (R) and absorption coefficient (α) for the different systems with parallel (left) and perpendicular (right) electric field. Shaded stripes represent the optical region.

tric field, new peaks with respect to G/IL [55] are found for Mg, Ca and Al at the same energies as for the dielectric function.

The complex refractive index compares the propagation of an electromagnetic wave in vacuum and in a given material. The optical refractive index, $n(\omega)$ (which represents the real part of the complex refractive index and is necessary for the optical devices), and the extinction coefficient, $\kappa(\omega)$ (which represents its imaginary part), as a function of energy can be both determined from the real and imaginary parts of the dielectric function as described in [69].

From Figs. 8 and S5, it can be seen that the refractive index has an anisotropic behavior. For parallel polarization the behavior observed for Li, Na and Al is similar to the one previously reported for the adsorption of K [69], with $n(\omega)$ reaching values close to zero in the lowest frequency interval of $[0, 1]$ eV. Mg shows similar characteristics, but its refractive index goes to zero at lower frequencies and it reaches a maximum value of 1.65 at 0.6 eV. For Ca, an intense peak of 9.5 is obtained at 0.06 eV and it seems to be the metal that modifies the least the shape of the curve that was observed for G/IL [69]. It must be noted that for energies larger than about 4 eV the refractive index value is less than one, due to the phase velocity of the electromagnetic field being higher than the speed of light in vacuum. The features for perpendicular polarization are similar for all the metals other than Mg, which shows the highest value (1.3) at 2.8 eV. In this case, the static refractive index at vanishing frequencies (i.e. $n(0)$), takes values of 1.04 for Li and Na, 1.07 for Mg and Al, and 1.13 for Ca, thus validating the relation $n(0) = \sqrt{\varepsilon_1(0)}$. These values point out that the mobility of electrons increases after adsorption of Ca compared to the other metals. Moreover, when a material exhibits a refractive index that varies based on the polarization of light, it is referred to as birefringent. In our systems, the difference between the parallel and perpendicular $n(\omega)$ is ca. 0.2 in the visible range, and prominent changes take place in the low-frequency region, specially for Ca.

Concerning the extinction coefficient, which indicates the degree of attenuation of the electromagnetic waves when propagating through the material, is as well clearly anisotropic. For the in-plane polarization, the adsorption of Mg causes the first minimum to move towards lower energies compared to Li, Na and Al, whereas doping with Ca shows the opposite effect. In addition, $\kappa(\omega)$ dramatically increases at low frequencies for all the metal atoms with respect to G/IL and it goes to zero when the frequency exceeds ~ 13 eV, in a similar way to what happens in the presence of K [69]. In the case of the out-of-plane polarization, the main difference arises again for Mg and Al, which show peaks at ~ 2.9 eV and in the region around 5 eV, respectively. Thus, we can state that different choices of the doping metal atom allow tuning the refractive index and the extinction coefficient in the low electron energy region for different applications.

Optical reflectivity (R) and absorption (α) coefficients were also calculated as detailed in [69] and analyzed in Figs. 8 and S5. Firstly, the reflectivity parameter shows prominent reflection at low frequencies for parallel incident electric field (from 0 to 0.4 eV for Mg, and from 0 to 1.1 eV for the rest of the metals). Then, in the visible range, R is shown to be below 20% and it vanishes at 7.6 eV. On the other hand, for perpendicular incident electric field the calculated reflectivity is zero in almost all the considered energy range, and it does not exceed a 5% in any case. Once again, Mg is the only metal atom that shows a peak within the visible range at 2.9 eV.

With regard to the absorption coefficient, it clearly follows the same behavior as the extinction coefficient. The results for the parallel polarization indicate that the absorption in the presence of all the metals starts at very low frequencies, and it increases at higher energies reaching a maximum value at around 4 eV. All the changes observed at low frequencies in the in-plane optical parameters with respect to the G/IL system [69] are due to the free electrons being the ones excited and contributing to optical transitions. The variation of the number of free electrons with metal-doping and the electron transfer process from the metal to graphene not only induce modifications in the electronic properties, but are also behind the effects observed in the near-zero frequency region for a parallel electric field. For perpendicular polarization, there is an overall increasing tendency for all the metals up to ~ 14.5 eV, before α starts to decrease. This is due to the bound electrons being able to oscillate with increasing frequency when increasing the energy of the incident electric field just up to a given value, after which the absorption process decreases. Looking at $\alpha(\omega)$ and $\kappa(\omega)$ we can confirm that these materials are transparent only for energies above 18 eV.

4. Conclusions

In this work, we employed plane wave DFT calculations to analyze how the electronic and optical properties of a graphene 2D surface are modified by the adsorption of an ionic liquid ([BMIM][BF_4]) mixed with a metal salt. Several metals of different valence and ionic radius (Li, Na, Mg, Ca, Al) were selected in order to shed some light on how the features of the systems are affected by these parameters.

A Bader charge analysis showed that most metals transfer 1 electron to the graphene surface, regardless of their valence. The ionization energy seems to be responsible for this behavior, as it prevents the electron exchange on Mg, the metal with the highest 1st IE, and induces the second electron transfer on Ca, whose 2nd IE is the lowest. This effect can also be observed in a structural analysis, where all the metals other than Mg are adsorbed near the 2D surface while sharing their electrons, with lithium adsorption being the most stable one and magnesium having the lowest binding energy.

From the charge density difference we confirmed that metal atoms acquired an electron loss configuration and carbon atoms around them showed gain of electrons. In addition, the redistribution of electric charge in the graphene surface was observed to be homogeneous with the adsorption of Na and Al, whereas the other metals induced high polarization in their neighboring carbon atoms. A band structure analysis showed that our system has two well differentiated parts: the 2D surface and the molecular complex, which is formed by the IL and the metal. The band structure of pristine graphene is conserved, but the Dirac cone is downshifted below the Fermi level as a consequence of the charge transfer. Moreover, new molecular levels arise in the system. The partial density of states also revealed some key differences between these systems. The metals that show more states close to the Dirac cone are Mg and Ca. However, the ionization of Mg is highly unlikely, which leads to its accommodation further from the surface.

Concerning the optical properties, all the magnitudes analyzed show an anisotropic behavior for the different polarizations of light. The adsorption of Mg and Ca leads to different features compared to the other metals, the former due to being positioned at great distances and the latter due to its larger charge transfer to graphene. Different plasma frequencies are induced depending on the metal at the interface for parallel polarization, whereas no collective excitations of the electrons for perpendicular polarization were found. Also, the analysis of the static refractive index showed that the mobility of the electrons is increased when Ca is adsorbed compared to the other metals.

We hope that this work will contribute to the current research on the possibility to tune the optoelectronic properties of graphene using ionic liquids and metal salts and provide a basis for the development of novel electrochemical and photonic devices. Further study employing more realistic electrodes such as metal oxide surfaces, and analyzing how the metal atom intercalation and alloy formation are affected by the findings reported in this work is now in progress.

CRediT authorship contribution statement

Alejandro Rivera-Pousa: Formal analysis, Investigation, Methodology, Software, Validation, Visualization, Writing – original draft, Writing – review & editing. **José M. Otero-Mato:** Formal analysis, Investigation, Methodology, Software, Validation, Writing – review & editing. **Carlos Damián Rodríguez-Fernández:** Formal analysis, Investigation, Methodology, Software, Validation, Writing – review & editing. **Kazem Zhour:** Formal analysis, Investigation, Methodology, Software, Validation, Writing – review & editing. **Hadrián Montes-Campos:** Conceptualization, Formal analysis, Investigation, Methodology, Project administration, Software, Supervision, Validation, Visualization, Writing – original draft, Writing – review & editing. **Trinidad Méndez-Morales:** Conceptualization, Formal analysis, Investigation, Methodology, Project administration, Software, Supervision, Validation, Visualization, Writing – original draft, Writing – review & editing. **Luis M. Varela:** Conceptualization, Formal analysis, Funding acquisition, Project administration, Supervision, Visualization, Writing – review & editing.

Declaration of competing interest

The authors declare that they have no known competing financial interests or personal relationships that could have appeared to influence the work reported in this paper.

Data availability

Data will be made available on request.

Acknowledgements

The financial support of the Spanish Ministry of Science and Innovation (PID2021-126148NA-I00 funded by MCIN/AEI/10.13039/501100011033/FEDER, UE) is gratefully acknowledged. Moreover, this work was funded by the Xunta de Galicia (GRC ED431C 2020/10). A. R.-P. and J.M.O.-M. thank the Spanish Ministry of Education for their FPU grants (FPU16/01500 and FPU18/01597). C. D. R. F. thanks the support of Xunta de Galicia through the grant ED481A-2018/032. T. M. M. acknowledges her contract funded by the pilot program of the USC for the recruitment of distinguished research personnel—call 2021 under the agreement between the USC and the Santander Bank for 2021–2024. H.M.C. thanks the USC for his “Convocatoria de Recualificación do Sistema Universitario Español-Margarita Salas” postdoctoral grant under the “Plan de Recuperación Transformación” program funded by the Spanish Ministry of Universities with European Union’s NextGenerationEU funds. This work was supported by the Fundação para a Ciência e a Tecnologia (FCT) (funded by national funds through the FCT/MCTES (PIDDAC)) to CIQUP, Faculty of Science, University of Porto (Project UIDB/00081/2020), IMS-Institute of Molecular Sciences (LA/P/0056/2020). Facilities provided by the Galician Supercomputing Centre (CESGA) are also acknowledged.

Appendix A. Supplementary material

Supplementary material related to this article can be found online at https://doi.org/10.1016/j.molliq.2023.123460.

References

[1] Z. Xie, B. Zhang, Y. Ge, Y. Zhu, G. Nie, Y. Song, C.-K. Lim, H. Zhang, P.N. Prasad, Chemistry, functionalization, and applications of recent monoelemental two-dimensional materials and their heterostructures, Chem. Rev. 122 (2022) 1127–1207.
[2] H. Qiao, H. Liu, Z. Huang, R. Hu, Q. Ma, J. Zhong, X. Qi, Tunable electronic and optical properties of 2d monoelemental materials beyond graphene for promising applications, Energy Environ. Mat. 4 (2021) 522–543.
[3] L.A. Falkovsky, Optical properties of graphene, J. Phys. Conf. Ser. 129 (2008) 012004.
[4] D.G. Papageorgiou, I.A. Kinloch, R.J. Young, Mechanical properties of graphene and graphene-based nanocomposites, Prog. Mater. Sci. 90 (2017) 75–127.
[5] A.H. Castro Neto, F. Guinea, N.M.R. Peres, K.S. Novoselov, A.K. Geim, The electronic properties of graphene, Rev. Mod. Phys. 81 (2009) 109–162.
[6] N.R. Abdullah, B.J. Abdullah, C.-S. Tang, V. Gudmundsson, Properties of bc6n monolayer derived by first-principle computation: influences of interactions between dopant atoms on thermoelectric and optical properties, Mater. Sci. Semicond. Process. 135 (2021) 106073.
[7] M. Rafique, Y. Shuai, I. Ahmed, R. Shaikh, M.A. Tunio, Tailoring electronic and optical parameters of bilayer graphene through boron and nitrogen atom co-substitution; an ab-initio study, Appl. Surf. Sci. 480 (2019) 463–471.
[8] G. Ambrosio, G. Drera, G.D. Santo, L. Petaccia, L. Daukiya, A. Brown, B. Hirsch, S.D. Feyter, L. Sangaletti, S. Pagliara, Interface chemistry of graphene/cu grafted by 3, 4,5-tri-methoxyphenyl, Sci. Rep. 10 (2020) 1–9.
[9] V. Kumar, R. Santosh, First-principle calculations of structural, electronic, optical and thermodynamical properties of fluorinated graphene, Mater. Sci. Eng. B 246 (2019) 127–135.
[10] M.Y. Hanna, I. Santoso, M.A.U. Absor, The role of the oxygen impurity on the electronic properties of monolayer graphene: a density-functional study, J. Phys. Conf. Ser. 1011 (2018) 012071.
[11] T. Sruthi, T. Kartick, Route to achieving enhanced quantum capacitance in functionalized graphene based supercapacitor electrodes, J. Phys. Condens. Matter 31 (2019) 475502.
[12] R. You, Y.-Q. Liu, Y.-L. Hao, D.-D. Han, Y.-L. Zhang, Z. You, Laser fabrication of graphene-based flexible electronics, Adv. Mater. 32 (2020) 1901981.
[13] A. Olabi, M.A. Abdelkareem, T. Wilberforce, E.T. Sayed, Application of graphene in energy storage device – a review, Renew. Sustain. Energy Rev. 135 (2021) 110026.
[14] S. Priyadarsini, S. Mohanty, S. Mukherjee, S. Basu, M. Mishra, Graphene and graphene oxide as nanomaterials for medicine and biology application, J. Nanostruct. Chem. 8 (2018) 123–137.
[15] Y. Qiao, X. Li, T. Hirtz, G. Deng, Y. Wei, M. Li, S. Ji, Q. Wu, J. Jian, F. Wu, et al., Graphene-based wearable sensors, Nanoscale 11 (2019) 18923–18945.
[16] F. Larki, Y. Abdi, P. Kameli, H. Salamati, An effort towards full graphene photodetectors, Photonic Sens. (2022) 1–37.
[17] S. Alvin, H.S. Cahyadi, J. Hwang, W. Chang, S.K. Kwak, J. Kim, Revealing the intercalation mechanisms of lithium, sodium, and potassium in hard carbon, Adv. Energy Mater. 10 (2020) 2000283.
[18] Y. Li, Y. Lu, P. Adelhelm, M.-M. Titirici, Y.-S. Hu, Intercalation chemistry of graphite: alkali metal ions and beyond, Chem. Soc. Rev. 48 (2019) 4655–4687.

[19] X. Liu, Y. Han, J.W. Evans, A.K. Engstfeld, R.J. Behm, M.C. Tringides, M. Hupalo, H.-Q. Lin, L. Huang, K.-M. Ho, et al., Growth morphology and properties of metals on graphene, Prog. Surf. Sci. 90 (2015) 397–443.
[20] S.K. Gupta, H.R. Soni, P.K. Jha, Electronic and phonon bandstructures of pristine few layer and metal doped graphene using first principles calculations, AIP Adv. 3 (2013) 032117.
[21] M. Xu, H. Wang, S. Sun, H. Li, X. Li, Y. Chen, Y. Ni, First-principles study of metal atoms adsorption on 2d dumbbell c4n, Phys. Status Solidi B 257 (2020) 1900205.
[22] M. Rafique, Y. Shuai, H.-P. Tan, M. Hassan, Manipulating intrinsic behaviors of graphene by substituting alkaline earth metal atoms in its structure, RSC Adv. 7 (2017) 16360–16370.
[23] A.C.F. Serraon, J.A.D. Del Rosario, P.-Y. Abel Chuang, M.N. Chong, Y. Morikawa, A.A.B. Padama, J.D. Ocon, Alkaline earth atom doping-induced changes in the electronic and magnetic properties of graphene: a density functional theory study, RSC Adv. 11 (2021) 6268–6283.
[24] K.T. Chan, J.B. Neaton, M.L. Cohen, First-principles study of metal adatom adsorption on graphene, Phys. Rev. B 77 (2008) 235430.
[25] S. Ullah, P.A. Denis, F. Sato, Adsorption and diffusion of alkali-atoms (li, na, and k) on ben dual doped graphene, Int. J. Quant. Chem. 119 (2019) e25900.
[26] A.P. Durajski, K.M. Skoczylas, R. Szczęśniak, Superconductivity in bilayer graphene intercalated with alkali and alkaline earth metals, Phys. Chem. Chem. Phys. 21 (2019) 5925–5931.
[27] C.S. Praveen, S. Piccinin, S. Fabris, Adsorption of alkali adatoms on graphene supported by the au/ni(111) surface, Phys. Rev. B 92 (2015) 075403.
[28] O. Farkad, R. Takassa, F. Elfatouaki, S. Hassine, Y. Ijdiyaou, E. Ibnouelghazi, D. Abouelaoualim, Structural, electronic and optical properties of ab bilayer graphene intercalated by sr atom: a first principles study, Diam. Relat. Mater. 126 (2022) 109082.
[29] T. Kaneko, R. Saito, First-principles study on interlayer state in alkali and alkaline earth metal atoms intercalated bilayer graphene, Surf. Sci. 665 (2017) 1–9.
[30] Y. Shuai, M. Rafique, M. Moazam Baloch, M. Ali Tunio, I. Ahmed, Dft study on tailoring the structural, electronic and optical properties of bilayer graphene through metalloids intercalation, Chem. Phys. 536 (2020) 110828.
[31] Z. Wang, S.M. Selbach, T. Grande, Van der Waals density functional study of the energetics of alkali metal intercalation in graphite, RSC Adv. 4 (2014) 4069–4079.
[32] E. Olsson, G. Chai, M. Dove, Q. Cai, Adsorption and migration of alkali metals (li, na, and k) on pristine and defective graphene surfaces, Nanoscale 11 (2019) 5274–5284.
[33] S. Pakhira, K.P. Lucht, J.L. Mendoza-Cortes, Dirac cone in two dimensional bilayer graphene by intercalation with v, nb, and ta transition metals, J. Chem. Phys. 148 (2018) 064707.
[34] S. Pakhira, J.L. Mendoza-Cortes, Tuning the Dirac cone of bilayer and bulk structure graphene by intercalating first row transition metals using first-principles calculations, J. Phys. Chem. C 122 (2018) 4768–4782.
[35] E. Kianfar, S. Mafi, Ionic liquids: properties, application, and synthesis, Fine Chem. Eng. (2021) 22–31.
[36] T. Welton, Ionic liquids: a brief history, Biophys. Rev. 10 (2018) 691–706.
[37] M.B. Shiflett, Commercial Applications of Ionic Liquids, vol. 605, Springer, 2020.
[38] H. Liu, H. Yu, Ionic liquids for electrochemical energy storage devices applications, J. Mater. Sci. Technol. 35 (2019) 674–686.
[39] D.R. MacFarlane, N. Tachikawa, M. Forsyth, J.M. Pringle, P.C. Howlett, G.D. Elliott, J.H. Davis, M. Watanabe, P. Simon, C.A. Angell, Energy applications of ionic liquids, Energy Environ. Sci. 7 (2014) 232–250.
[40] G. Kaur, H. Kumar, M. Singla, Diverse applications of ionic liquids: a comprehensive review, J. Mol. Liq. (2022) 118556.
[41] A.J. Greer, J. Jacquemin, C. Hardacre, Industrial applications of ionic liquids, Molecules 25 (2020) 5207.
[42] Q. Gao, Y. Zhang, S. Xu, A. Laaksonen, Y. Zhu, X. Ji, X. Lu, Physicochemical properties and structure of fluid at nano-/micro-interface: progress in simulation and experimental study, in: SI: Molecular Thermodynamics for Green Engineering, Green Energy Environ. 5 (2020) 274–285.
[43] S. Aldroubi, N. Brun, I. Bou Malham, A. Mehdi, When graphene meets ionic liquids: a good match for the design of functional materials, Nanoscale 13 (2021) 2750–2779.
[44] P. Snapp, J.M. Kim, C. Cho, J. Leem, M.F. Haque, S. Nam, Interaction of 2d materials with liquids: wettability, electrochemical properties, friction, and emerging directions, NPG Asia Mater. 12 (2020) 1–16.
[45] R. Talaei, B. Khalili, M. Mokhtary, Modulation of opto-electronic properties of the functionalized hexagonal boron nitride nanosheets with tunable aryl alkyl ionic liquids (taails): defect based analysis, J. Mol. Liq. 304 (2020) 112696.
[46] V. Anithaa, R. Shankar, S. Vijayakumar, Structural and electronic properties of graphene and its derivatives physisorbed by ionic liquids, Diam. Relat. Mater. 109 (2020) 108005.
[47] C. Herrera, R. Alcalde, M. Atilhan, S. Aparicio, Theoretical study on amino acid-based ionic pairs and their interaction with carbon nanostructures, J. Phys. Chem. C 118 (2014) 9741–9757.
[48] M. Shyama, S. Lakshmipathi, Adsorption properties of amino acid-based ionic liquids (aails) on edge fluorinated graphene surface–a dft study, Mol. Simul. 47 (2021) 1066–1077.
[49] Y. He, Y. Guo, F. Yan, T. Yu, L. Liu, X. Zhang, T. Zheng, Density functional theory study of adsorption of ionic liquids on graphene oxide surface, Chem. Eng. Sci. 245 (2021) 116946.
[50] A. Ruzanov, M. Lembinen, H. Ers, J.M. Garcia de la Vega, I. Lage-Estebanez, E. Lust, V.B. Ivanistsev, Density functional theory study of ionic liquid adsorption on circumcoronene shaped graphene, J. Phys. Chem. C 122 (2018) 2624–2631.
[51] D. Wagle, G. Kamath, G.A. Baker, Elucidating interactions between ionic liquids and polycyclic aromatic hydrocarbons by quantum chemical calculations, J. Phys. Chem. C 117 (2013) 4521–4532.
[52] T.P.C. Klaver, M. Luppi, M.H.F. Sluiter, M.C. Kroon, B.J. Thijsse, Dft study of 1, 3-dimethylimidazolium tetrafluoroborate on al and cu(111) surfaces, J. Phys. Chem. C 115 (2011) 14718–14730.
[53] H. Valencia, M. Kohyama, S. Tanaka, H. Matsumoto, Ab initio study of emim-bf 4 crystal interaction with a li (100) surface as a model for ionic liquid/li interfaces in li-ion batteries, J. Chem. Phys. 131 (2009) 244705.
[54] C. Wei, K. Jiang, T. Fang, X. Liu, Effects of anions and alkyl chain length of imidazolium-based ionic liquids at the au (111) surface on interfacial structure: a first-principles study, Green Chem. Eng. 2 (2021) 402–411.
[55] K. Zhour, J.M. Otero-Mato, F.E.H. Hassan, H. Fahs, M. Vaezzadeh, E. López-Lago, L.J. Gallego, L.M. Varela, Electronic and optical properties of borophene and graphene with an adsorbed ionic liquid: a density functional theory study, J. Mol. Liq. 316 (2020) 113803.
[56] L. Zhu, A. Fu, The influence of ionic liquids adsorption on the electronic and optical properties of phosphorene and arsenene with different phases: a computational study, Molecules 27 (2022) 2518.
[57] M. Shakourian-Fard, Z. Jamshidi, A. Bayat, G. Kamath, Meta-hybrid density functional theory study of adsorption of imidazolium- and ammonium-based ionic liquids on graphene sheet, J. Phys. Chem. C 119 (2015) 7095–7108.
[58] M. Shakourian-Fard, G. Kamath, The effect of defect types on the electronic and optical properties of graphene nanoflakes physisorbed by ionic liquids, Phys. Chem. Chem. Phys. 19 (2017) 4383–4395.
[59] M. Shakourian-Fard, S.M. Taimoory, V. Semeniuchenko, G. Kamath, J.F. Trant, The effect of ionic liquid adsorption on the electronic and optical properties of fluorographene nanosheets, J. Mol. Liq. 268 (2018) 206–214.
[60] R. Bari, G. Tamas, F. Irin, A.J. Aquino, M.J. Green, E.L. Quitevis, Direct exfoliation of graphene in ionic liquids with aromatic groups, Colloids Surf. A, Physicochem. Eng. Asp. 463 (2014) 63–69.
[61] G. García, M. Atilhan, S. Aparicio, In silico rational design of ionic liquids for the exfoliation and dispersion of boron nitride nanosheets, Phys. Chem. Chem. Phys. 18 (2016) 1212–1224.
[62] M. Shakourian-Fard, G. Kamath, Z. Jamshidi, Trends in physisorption of ionic liquids on boron-nitride sheets, J. Phys. Chem. C 118 (2014) 26003–26016.
[63] G. García, M. Atilhan, S. Aparicio, Adsorption of choline benzoate ionic liquid on graphene, silicene, germanene and boron-nitride nanosheets: a dft perspective, Phys. Chem. Chem. Phys. 17 (2015) 16315–16326.
[64] M. Lalitha, S. Lakshmipathi, Interface energetics of $[Emim]^+[X]^-$ and $[Bmim]^+[X]^-$ ($X = BF_4$, Cl, PF_6, TfO, Tf_2N) based ionic liquids on graphene, defective graphene, and graphyne surfaces, J. Mol. Liq. 236 (2017) 124–134.
[65] Y. Lu, Y. Hong, Z. Xu, H. Liu, Interfacial interactions and structures of imidazolium-based ionic liquids on black phosphorus surface from first-principles, J. Mol. Liq. 335 (2021) 116562.
[66] Y. Lu, Y. Xu, L. Lu, Z. Xu, H. Liu, Interfacial interactions and structures of protic ionic liquids on a graphite surface: a first-principles study and comparison with aprotic ionic liquids, Phys. Chem. Chem. Phys. 23 (2021) 18338–18348.
[67] M. Shakourian-Fard, H.R. Ghenaatian, G. Kamath, S.M. Taimoory, Unraveling the effect of nitrogen doping on graphene nanoflakes and the adsorption properties of ionic liquids: a dft study, J. Mol. Liq. 312 (2020) 113400.
[68] Y. Tang, W. Huai, H. Li, X. Mao, J. Xie, J.Y. Lee, A. Fu, Adsorption of [bf4]- anion-based ionic liquids on phosphorene, arsenene, and antimonene: a density functional theory study, Int. J. Quant. Chem. 121 (2021) e26668.
[69] K. Zhour, J.M. Otero-Mato, F.E.H. Hassan, H. Fahs, M. Vaezzadeh, E. López-Lago, L.J. Gallego, L.M. Varela, Tuning the hybrid borophene-/graphene-ionic liquid interface: effect of metal cations on the electronic and photonic properties, J. Mol. Liq. 321 (2021) 114759.
[70] B. Mandal, S. Chakrabarti, A.K. Thakur, Dft simulation of nafesno4 structure, electronic and electrochemical properties validated by experimental results, Comput. Mater. Sci. 192 (2021) 110401.
[71] A.H. Mashhadzadeh, M. Ghanbari, A. Koochaki, S. Seyyedbarzegar, M.G. Ahangari, Experiment and theory for acetylene adsorption in transformer oil, J. Mol. Struct. 1230 (2021) 129860.
[72] H.M. Coromina, B. Adeniran, R. Mokaya, D.A. Walsh, Bridging the performance gap between electric double-layer capacitors and batteries with high-energy/high-power carbon nanotube-based electrodes, J. Mater. Chem. A 4 (2016) 14586–14594.
[73] M.-C. Liu, C. Lu, Y. Xu, Y.-X. Hu, J. Li, H. Zhang, Y.-S. Zhang, B.-M. Zhang, L.-B. Kong, W.-W. Liu, et al., Three-dimensional interconnected reticular porous carbon from corn starch by a sample sol–gel method toward high-performance supercapacitors with aqueous and ionic liquid electrolytes, ACS Sustain. Chem. Eng. 7 (2019) 18690–18699.
[74] P. Giannozzi, S. Baroni, N. Bonini, M. Calandra, R. Car, C. Cavazzoni, D. Ceresoli, G.L. Chiarotti, M. Cococcioni, I. Dabo, et al., Quantum espresso: a modular and open-source software project for quantum simulations of materials, J. Phys. Condens. Matter 21 (2009) 395502.

[75] P. Giannozzi, O. Andreussi, T. Brumme, O. Bunau, M.B. Nardelli, M. Calandra, R. Car, C. Cavazzoni, D. Ceresoli, M. Cococcioni, et al., Advanced capabilities for materials modelling with quantum espresso, J. Phys. Condens. Matter 29 (2017) 465901.
[76] P. Giannozzi, O. Baseggio, P. Bonfà, D. Brunato, R. Car, I. Carnimeo, C. Cavazzoni, S. De Gironcoli, P. Delugas, F. Ferrari Ruffino, et al., Quantum espresso toward the exascale, J. Chem. Phys. 152 (2020) 154105.
[77] J.P. Perdew, K. Burke, M. Ernzerhof, Generalized gradient approximation made simple, Phys. Rev. Lett. 77 (1996) 3865.
[78] V. Gomez-Gonzalez, J.M. Otero-Mato, H. Montes-Campos, X. Garcia-Andrade, A. Garcia-Fuente, A. Vega, J. Carrete, O. Cabeza, L.J. Gallego, L.M. Varela, Borophene vs. graphene interfaces: tuning the electric double layer in ionic liquids, J. Mol. Liq. 303 (2020) 112647.
[79] M. Methfessel, A. Paxton, High-precision sampling for Brillouin-zone integration in metals, Phys. Rev. B 40 (1989) 3616.
[80] F. Zhang, B. Sahu, H. Min, A.H. MacDonald, Band structure of a b c-stacked graphene trilayers, Phys. Rev. B 82 (2010) 035409.
[81] A.R. Botello-Mendez, S.M.-M. Dubois, A. Lherbier, J.-C. Charlier, Achievements of dft for the investigation of graphene-related nanostructures, Acc. Chem. Res. 47 (2014) 3292–3300.
[82] J.A. Fürst, J.G. Pedersen, C. Flindt, N.A. Mortensen, M. Brandbyge, T.G. Pedersen, A.-P. Jauho, Electronic properties of graphene antidot lattices, New J. Phys. 11 (2009) 095020.
[83] S. Paavilainen, M. Ropo, J. Nieminen, J. Akola, E. Rasanen, Coexisting honeycomb and Kagome characteristics in the electronic band structure of molecular graphene, Nano Lett. 16 (2016) 3519–3523.
[84] G. Gui, J. Li, J. Zhong, Band structure engineering of graphene by strain: first-principles calculations, Phys. Rev. B 78 (2008) 075435.
[85] R.F.W. Bader, Atoms in molecules, Acc. Chem. Res. 18 (1985) 9–15.
[86] D.R. Lide, CRC Handbook of Chemistry and Physics, 84th edition, CRC Press, 2003.
[87] Z.H. Zhu, G.Q. Lu, Comparative study of li, na, and k adsorptions on graphite by using ab initio method, Langmuir 20 (2004) 10751–10755.
[88] V. Gómez-González, A. Garcìa-Fuente, A. Vega, J. Carrete, O. Cabeza, L. Gallego, L. Varela, Density functional study of charge transfer at the graphene/ionic liquid interface, J. Phys. Chem. C 122 (2018) 15070–15077.
[89] B.A. Boukamp, A linear Kronig-Kramers transform test for immittance data validation, J. Electrochem. Soc. 142 (1995) 1885.
[90] P. Nath, S. Chowdhury, D. Sanyal, D. Jana, Ab-initio calculation of electronic and optical properties of nitrogen and boron doped graphene nanosheet, Carbon 73 (2014) 275–282.
[91] F. Wooten, Optical Properties of Solids, Citeseer, 1972.
[92] S. Chowdhury, A. Majumdar, D. Jana, Electronic and optical properties of the supercell of 8-pmmn borophene modified on doping by h, li, be, and c: a dft approach, Appl. Phys. A 125 (2019) 1–14.